



Shahrood University of  
Technology



Iranian Society of  
Mining Engineering  
(IRSM)

## Three-Dimensional Elasto-Plastic Analysis of Delhi Metro Underground Tunnels under Seismic Loading

Rahul Shakya, and Manendra Singh\*

Department of Civil Engineering, National Institute of Technology Hamirpur, Himachal Pradesh, India

### Article Info

Received 10 July 2023

Received in Revised form 5  
November 2023

Accepted 10 December 2023

Published online 10 December  
2023

DOI: [10.22044/jme.2023.13348.2455](https://doi.org/10.22044/jme.2023.13348.2455)

### Keywords

Underground Tunnel

FEM

PLAXIS 3D

DMRC

### Abstract

Due to the critical nature of seismic risk in metro tunnels, the seismic response of underground tunnels is a highly delicate topic. The seismic response of a sub-surface structure depends more on the properties of the surrounding ground and the induced earth deformation during an earthquake than on the structure's inertial properties. This paper examines the seismic response of a typical section of the underground tunnel of Delhi Metro Rail Corporation (DMRC) between Rajiv Square and Patel Square in New Delhi's Connaught Place. Three-dimensional elasto-plastic analysis of Delhi metro underground tunnels under the seismic loading has been performed by finite element method using the Plaxis 3D software. Additionally, the influence of various boundary conditions on the dynamic response of metro tunnels has been examined. A comparison of the three-dimensional analysis with the two-dimensional plane-strain analysis has also been made. Horizontal displacements were experienced maximum compared to the longitudinal and vertical displacements in the soil-tunnel system. In dynamic analysis, the absorbent boundary is much more effective in controlling the displacements and the induced acceleration than the elementary boundary or the free-field boundary.

### 1. Introduction

The world is currently grappling with the significant issue of population expansion. The population of most nations worldwide is rapidly increasing. The growth of the population has a significant impact on people's living standards. Thus, urbanization increases to accomplish their requirements for a better livelihood. Urbanization is when the population shifts from rural to urban areas due to various factors. Major contributors to urbanization include the rise of industry and commerce; the shift from rural to urban lifestyles; the expansion of economic and social opportunities; and the spread of public services. As cities have expanded, so has the demand for ground space. The above-ground space in any city is limited. To fulfil all demands (developed as a result of urbanization), the sub-surface structure becomes more efficient for fulfilling these requirements. Sub-surface structures are extremely useful in transportation such as underground tunnels for the

mass rapid transit system, the water conductor system of hydropower projects, roadway and railway tunnels in hilly terrain, and underground gas and petroleum storage. Underground power plants, large storage facilities for solid or liquid fuels, underground structures for the protection of people or sensitive equipment, and various underground lifeline systems all play an increasingly important role in the modern economic and social development of a nation's economy and society. These structures must be designed to withstand dynamic loads from the outside or from within, as well as the effects of seismic waves. The study becomes more difficult due to the interactions of sub-surface structure with the surrounding soil, especially in dynamic conditions. This is likely why there is not as much written about the dynamic behavior of underground structures as there is about those above ground. Historically, the first studies on the dynamic

✉ Corresponding author: [manendra@nith.ac.in](mailto:manendra@nith.ac.in) (M. Singh)

analysis and design of underground structures had to do with underground nuclear shelters [1-3]. However, a great interest was created very quickly in the dynamic analysis and design of other underground structures such as tunnels and pipelines, which generally are less affected by seismic motion than surface structures. Li *et al.* [4] conducted a three-dimensional numerical investigation of the longitudinal seismic response of tunnels subjected to an asynchronous wave input. In this research work, the authors estimated free field motion using a one-dimensional time-domain method. With this wave-input method, a three-dimensional model of how soil and tunnel structures interact was made to predict how tunnels will move along their lengths during earthquakes that happen at different times. The findings demonstrated the feasibility of simulating the seismic response of an indefinitely long tunnel by using a computer model that was relatively long in the longitudinal direction. Varma *et al.* [5] have conducted a numerical analysis using the 2-dimensional distinct element modeling method to comprehend the behavior of a rock tunnel with joints under seismic loading to demonstrate that the linings of shallow-buried tunnels are more susceptible to deterioration under seismic stresses. To assess the stability of a shallow tunnel in soft ground, Imteyaz, W. and Mishra, S [6] utilize the FEM-based software, and concluded that the deeper tunnels exhibit enhanced stability under seismic conditions, despite variations in earthquake characteristics. Zaid, M. *et al.* [7] conducted a study to analyse the behaviour of urban tunnels under static loading conditions by using the finite element method. Singh *et al.* [8] conducted a case study of Delhi metro underground tunnels, and studied their dynamic response due to the Chamoli 1999 earthquake. Shah, I. A. and Zaid, M. [9] analyse the behaviour of an underground tunnel under varying levels of seismic loading using finite element analysis. The study highlights the importance of considering the magnitude of earthquakes for which the tunnel is being designed based on the past earthquake history of the region. Olarewaju *et al.* [10] explore underground pipe responses to blast loads, covering components like blast, ground, and interaction. It suggests numerical approaches, favouring them over analytical methods due to their broader applicability, and discusses the central difference and finite element methods for solving dynamic equations. Alzabeebee, S. [11] talks about the seismic settlement of shallow foundations built on sandy soil in earthquake prone areas. Many other

authors Stamos *et al.* [12, 13], Yu *et al.* [14, 15], Chen *et al.* [16], Ishimura *et al.* [17], Chun *et al.* [18], Li *et al.* [19] have also investigated the three-dimensional seismic behaviour of underground tunnels.

The Delhi Metro Rail Corporation (DMRC) has built and opened most major metro lines. The expansion of this network into the National Capital Region (NCR) is now underway. Based on India's earthquake zoning map, Delhi is in zone IV. The several DMRC tunnels below the ground are relatively shallow, and could be damaged in a large earthquake. Consequently, it is crucial to investigate whether damage occurs in this soil excavated tunnels and to comprehend how these buildings respond to earthquakes. Tunnels and underground structures, more generally, have a very different seismic response from that of above-ground structures due to the overall mass of the structure being typically small in proportion to the surrounding soil's mass. The response of an underground structure to this kind of event depends greatly on the induced ground deformation. The response of the ground around the structure and the imposed ground deformation are more important than the structure's inertia properties.

## 2. Problem Definition

Between Rajiv Square and Patel Square in Connaught Place, New Delhi, a representative section of the tunnels operated by the Delhi Metro Rail Corporation (DMRC) has been analysed in the analysis. The DMRC tunnel is 6.0 m in diameter and has an overburden depth of 2D (12.0 m). Liners made of 0.28 meter thick Reinforced Concrete (RC) have been installed as a support system. The Poisson's ratio of RC liners is 0.15, while the elastic modulus,  $E_c$ , is  $3.16 \times 10^7$  kPa. The average tunnel length was estimated to be 50.0 m. The RC linings have a 2% damping ratio. Table 1 displays the tunnel section's geometrical features. The DMRC tunnels have been excavated through alluvium deposits that are commonly referred as Delhi silt. The soil's behaviour has been modelled as elastoplastic, and the soil's productivity has been measured using the Mohr-Coulomb yield criterion. Table 2 and Table 3 show the depth dependence of the elastic modulus and geometric properties of the surrounding soil, respectively. The tunnel was dug without hitting any water table. In the present study, only the horizontal component of the Chamoli earthquake has been taken for dynamic analysis.

**Table 1. Geometrical specifications of Delhi metro tunnel [20, 21].**

Properties	Values
Tunnel's diameter, $D$	6.0 m
Depth of tunnel, $H$	2D (12 m)
Tunnel's length, $L$	50 m
Type of support system	Segmental Reinforced Concrete (RC) liners
RC liner's thickness	0.28 m
RC liner's Elastic modulus $E_c$	$3.16 \times 10^7$ kPa
Poisson's ratio (RC liners)	0.15
Damping ratio	2.0%

**Table 2. Elastic modulus variation of Delhi silt with depth [20, 21].**

Depth (m)	Thickness (m)	Elastic modulus (kPa)
0-10	10	$7.5 \times 10^3$
10-20	10	$15 \times 10^3$
20-35	15	$30 \times 10^3$
35-50	15	$40 \times 10^3$
50-60	10	$50 \times 10^3$

**Table 3. Properties of soil medium surrounding the tunnel [20, 21].**

Properties	Values
Unit weight of the soil, $\gamma_{bulk}$	18 kN/m <sup>3</sup>
Saturated unit weight of the soil, $\gamma_{sat}$	20 kN/m <sup>3</sup>
Cohesion, $c$	0
Friction angle, $\varphi$	35°
Dilatational angle, $\psi$	5°
Poisson's ratio	0.25
Damping ratio	15.0%

### 3. Numerical modelling

In this study, analysis was performed by using the FEM software Plaxis 3D to examine the metro tunnel's reaction to the earthquake. After performing a sensitivity analysis, a model size of 200 m x 50 m x 60 in the X, Y, and Z axes has been used in this study.

#### 3.1. Damping for soil and tunnel

While PLAXIS allows the users to model dynamic loading and vibrations, it doesn't provide built-in features for simulating damping directly. Instead, it relies on users to input appropriate dynamic properties including damping based on the material properties and analysis requirements. In the present analysis, damping was incorporated through Rayleigh damping.

Rayleigh damping is a common approach to model damping in dynamic analysis. It involves a combination of mass-proportional damping and stiffness-proportional damping. The users can specify the damping ratios for both mass and stiffness terms based on the characteristics of the

material and the structure. Rayleigh damping is calculated using the following Equation (1).

$$C = \alpha M + \beta K \quad (1)$$

where  $M$  and  $K$  are mass and stiffness matrices, and  $\alpha$  and  $\beta$  are the Rayleigh damping coefficients, which are determined by using the Equation 2.

$$\begin{Bmatrix} \alpha \\ \beta \end{Bmatrix} = \frac{2\zeta}{w_m + w_n} \begin{Bmatrix} w_m w_n \\ 1 \end{Bmatrix} \quad (2)$$

The damping ratio ( $\zeta$ ) characterizes the damping of vibrations, while the natural frequencies of the soil mass ( $\omega_m$  and  $\omega_n$ ) correspond to the mode shapes labelled as 'm' and 'n'. It is important to note that the structure and soil mass exhibit distinct modes of vibration. In this context, the specific values chosen for 'm' and 'n' are 1 and 2, respectively, indicating that the soil-tunnel system is considered to vibrate exclusively in modes 1 and 2. The damping coefficients  $\alpha$  and  $\beta$  were determined for both RC liners and the surrounding soil using Equations 1 and 2 [22].

### 3.2. Modelling of soil

Tetrahedral elements with 10 nodes and an average size of 16.16 m were considered after sensitivity analysis to model the soil domain. The elastoplastic behaviour of soil was considered in this analysis. Since soil is a non-linear material, it cannot be simulated using a linear elastic model; therefore, the Mohr-Coulomb model has been used for simulating the behaviour of surrounding soil. In the Mohr-Coulomb model, plasticity is associated with the development of irreversible strains, and it limits allowable stress states. The basic principle of elasto plasticity is that strains and strain rates are decomposed into an elastic part and a plastic part. The Mohr Coulomb model necessitates five parameters, typically well-known to geotechnical engineers, and they can be derived from fundamental soil sample tests. These essential parameters encompass Young's modulus, Poisson's ratio, friction angle, cohesion, and dilatancy angle [22].

### 3.3. Modelling of tunnel

Segmental RC liners were simulated by 6-noded triangular plate bending elements. A linear elastic model has been used for simulating the stress-strain behaviour of underground tunnels. The seismic response of an underground structure is primarily governed by the reactions of the surrounding ground and the applied ground deformation, rather than being dictated by the tunnel's inertial properties. This dependence on induced ground deformation drives the significance of considering the tunnel's linear behaviour in such cases. This entails the utilization of two key parameters – Elastic modulus (E) and Poisson's ratio ( $\nu$ ) to effectively model the tunnel's linear behaviour. The stress-strain relationship in the linear elastic model conforms to the principles of the generalised Hooke's law.

### 3.4. Interface condition

The assumption has been made that there will be no slipping between the tunnel and the soil medium that surrounds it. This simplification is commonly used in tunnel analysis because the sliding interface can introduce additional complexities and difficulties in analysis. There might be some degree of movement or interaction between the tunnel and the surrounding medium, but the assumption of no-slipping helps simplify the calculations and understanding of the tunnel behaviour. In soil-structure interaction (SSI) modeling, the concepts of no-slip and full-slip

conditions are applied to understand how soil and structures interact with each other. In this modeling, the authors use the interface element at the interface of the soil and the tunnel. The interface properties are dependent on the parameter  $R_i$  (reduction factor) and are given by the following equations [23]:

$$C_i = R_i * C_{soil} \quad (3)$$

$$\phi_i = \tan^{-1}(R_i \tan \phi_{soil}) \quad (4)$$

$$\psi_i = \begin{cases} 0 & R_i < 1 \\ \psi_{soil} & R_i = 1 \end{cases} \quad (5)$$

$$G_i = R_i^2 * G_{soil} \quad (6)$$

where  $C_{soil}$  = soil cohesion,  $\phi_{soil}$  = soil friction angle,  $G_{soil}$  = soil shear modulus, and  $\psi_{soil}$  = soil dilatancy. For a no slip condition,  $R_i$  as 1.0. As  $R_i$  reduces, relative slip between soil and tunnel liner is allowed. If  $R_i$  is zero, then no slip condition is simulated. From the analysis, the seismic response was found to be maximum for no slip condition therefore no slip condition was simulated between the soil and tunnel in this study.

### 3.5. Boundary conditions

For static response, nodes along the XZ plane of the model were constrained in the Y-direction while remaining free to move in the X- and Z-directions. Similarly, nodes along the YZ-plane of the model were constrained in the X-direction while remaining free to move in the Y and Z-directions. Top surface freedom was maintained in all directions, while bottom boundary freedom was enforced in all directions. Lysmer and Kuhlmeyer [24] suggested a viscous absorbent boundary to represent the displacement condition in dynamic analysis, and this boundary was implemented in both the horizontal and vertical directions (XZ and YZ planes) for dynamic analysis.

### 3.6. Earthquake loading

Only the horizontal component of the 1999 Chamoli earthquake that occurred in the lower Himalayas has been considered for seismic analysis. For the purpose of earthquake resistant analysis and the design of structures, realistic ground motion is required. In numerous cases, acquiring strong motion records at a specific site can be challenging and even if such records are accessible, there's no reliable basis to assume that a future earthquake would result in the same or similar ground motion. The chosen time history

needs to accurately represent the anticipated ground motion at the site, particularly the motion that would trigger the highest potential damage to the structure. Consequently, it's crucial to generate synthetic time histories for a specific site in order to predict a structure's earthquake response. The time history of the earthquake should be such that it can match the expected earthquake in that zone or for that site [25]. Thus, keeping this in mind, attempt was made to generate response spectra compatible with the time history for Delhi zone by using some of the available software packages. Since no major earthquake has occurred in Delhi city, therefore Chamoli (1999) earthquake of lower

Himalaya has been chosen for analysis. Chamoli (1999) earthquake occurred in the Chamoli district of Garhwal Himalaya, which exists in zone-V of the earthquake zoning map of India. However, Delhi falls in zone-IV on this map. Therefore, artificial time history must be generated for zone IV. Taking magnitude from target spectra (Figure 1a) and phase from given input history (Figure 1b), response spectra-compatible time history (Figure 1c) has been generated using Siesmo Match Software. The phase and time interval of the modified time history are same as the actual earthquake.

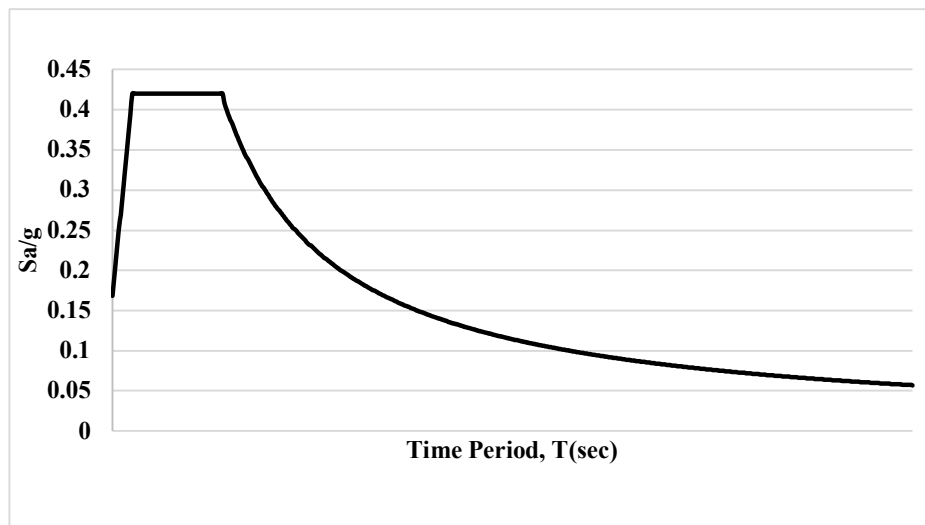


Figure 1a. Response spectra for zone IV (medium soil) for 15% damping ratio (IS:1893, Part - I, 2002).

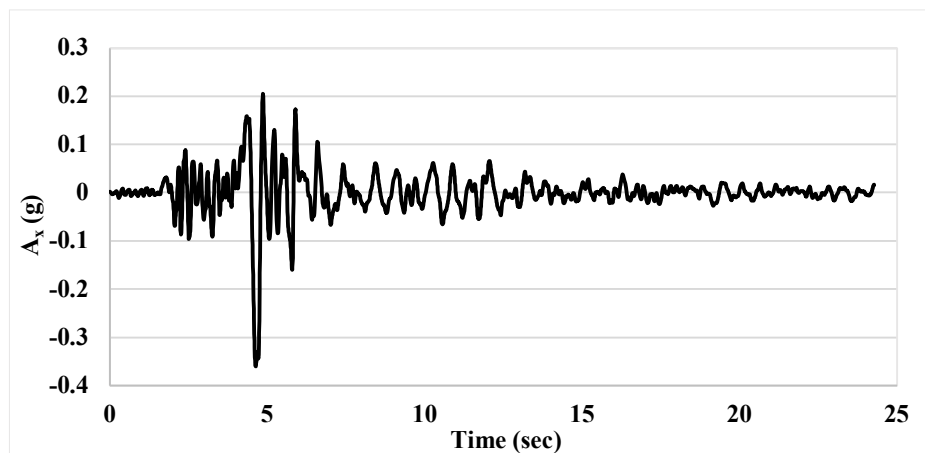


Figure 1b. Horizontal acceleration ( $A_x$ ) - time history of 1999 Chamoli earthquake.

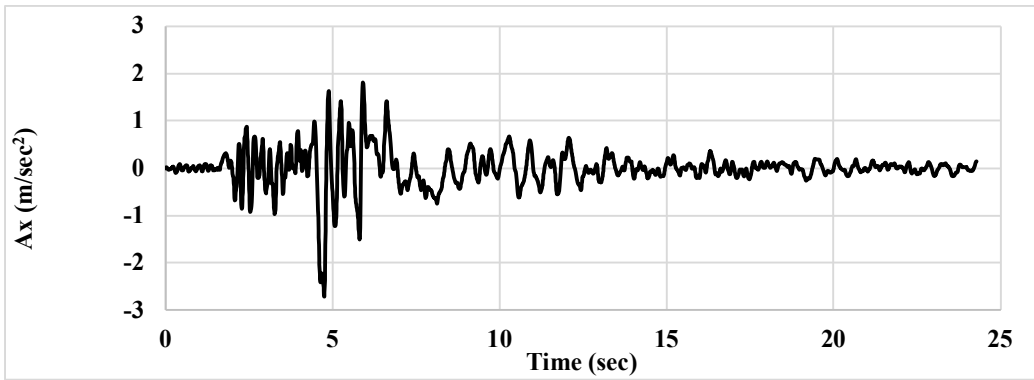


Figure 1c. Response spectra compatible time history for horizontal component of 1999 Chamoli earthquake.

**4. Results and Discussions**

**4.1. Deformed mesh**

Figure 2 depicts the deformed mesh after the end of the earthquake. The total displacement was 163.5 mm after the earthquake in element 1175 at node 7231. The total displacement are the

accumulated displacements at all nodes at the end of the simulation. If the displacement was found to be minimum near the space ground, it may happen due to the accumulation of all negative and positive displacement. Figure 2 shows the residual displacement, therefore, there is no significant change in the displacement seen around the tunnel.

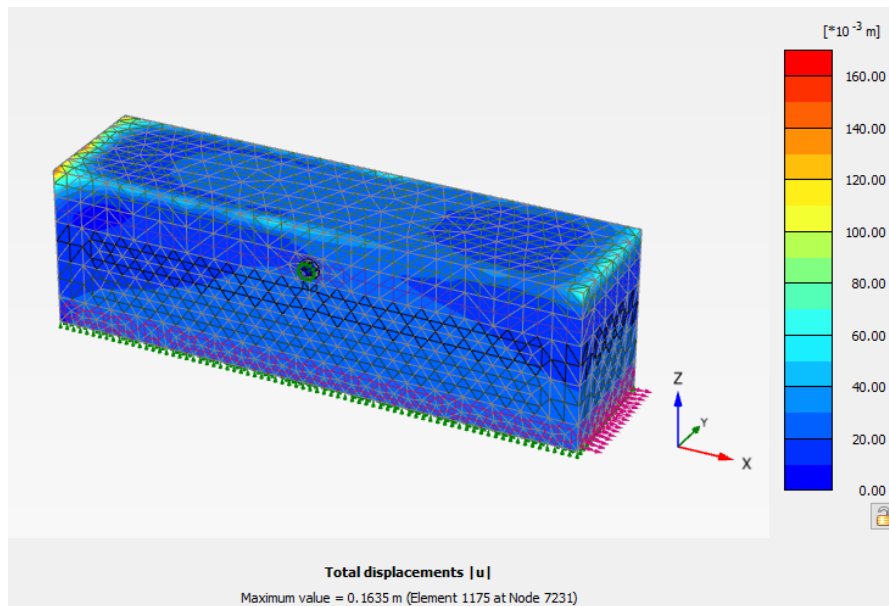


Figure 2. Deformed mesh after the earthquake.

**4.2. Horizontal displacements**

Figure 3 shows the horizontal displacement contours after the end of earthquake. The maximum horizontal displacement value is 71.36 mm in element 1032 at node 1162.

The values of maximum dynamic response, horizontal displacement ( $U_x$ ), vertical displacement ( $U_z$ ), longitudinal displacement ( $U_y$ ), horizontal acceleration ( $A_x$ ) at the ground surface, crown, invert, and springing points are summarised in Table 4. These values have been felt for the

horizontal component of the Chamoli earthquake (Figure 1c). The ground surface has experienced maximum horizontal displacement, which is 203.40 mm, whereas critical locations like a crown, invert, and the springing points undergo almost the same horizontal displacement. The other two displacements are negligible. Figure 4 shows the time history of horizontal displacement for specific points. After the earthquake, the data showed a residual horizontal displacement of around 21 mm at all critical locations.

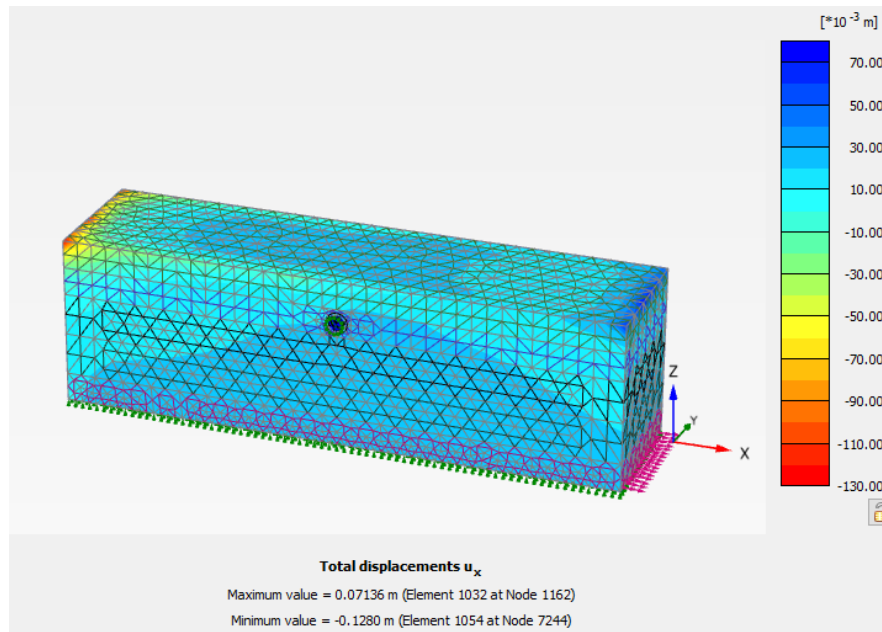


**Figure 3. Horizontal displacement contours after the earthquake.**

**Table 4. Dynamic response at critical locations due to the T component of earthquake.**

Critical locations	Coordinates	$A_x$ (m/s <sup>2</sup> )	$U_x$ (mm)	$U_y$ (mm)	$U_z$ (mm)
Ground surface	(0, 0, 0)	0.65	163.74	32	32
	(0, 25, 0)	1.19	203.40	1.14	0.36
Crown	(0, 50, 0)	0.60	155.17	41.27	34
	(0, 0, -12)	0.74	185.49	0	0.41
	(0, 25, -12)	0.79	187.37	0.07	0.31
	(0, 50, 12)	0.63	185.72	0.36	0.67
Invert	(0, 0, -18)	0.71	184.62	0	0.62
	(0, 25, -18)	0.95	184.57	0.02	0.41
	(0, 50, -18)	0.79	184.25	0.07	0.58
Springing point (1)	(3, 0, -15)	0.69	186.12	0	3.35
	(3, 25, -15)	0.82	185.36	0.03	2.89
	(3, 50, -15)	0.70	185.89	0	3.18
Springing point (2)	(-3, 0, -15)	0.69	184.40	0	2.87
	(-3, 25, -15)	0.82	185.73	0.03	2.66
	(-3, 50, -15)	0.69	185.87	0	2.98

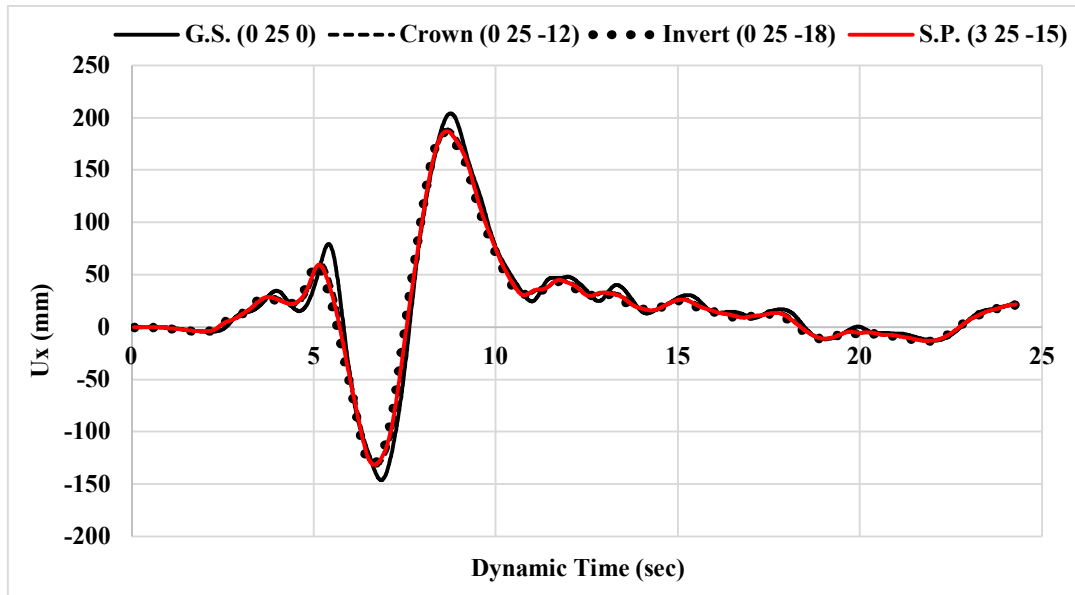


Figure 4. Horizontal displacement vs. time history at the different points.

### 4.3. Vertical displacements

Figure 5 shows the vertical displacement (in Z-direction) contours after the end of the earthquake. The maximum value of vertical displacement is 102.8 mm. Table 4 indicates that vertical displacement is significant only at the ground

surface, whereas the values at other critical locations are practically very small or negligible. The time history of vertical displacement at typical locations has been depicted in Figure 6, which shows that vertical displacement values do not change much concerning time except at the ground surface.

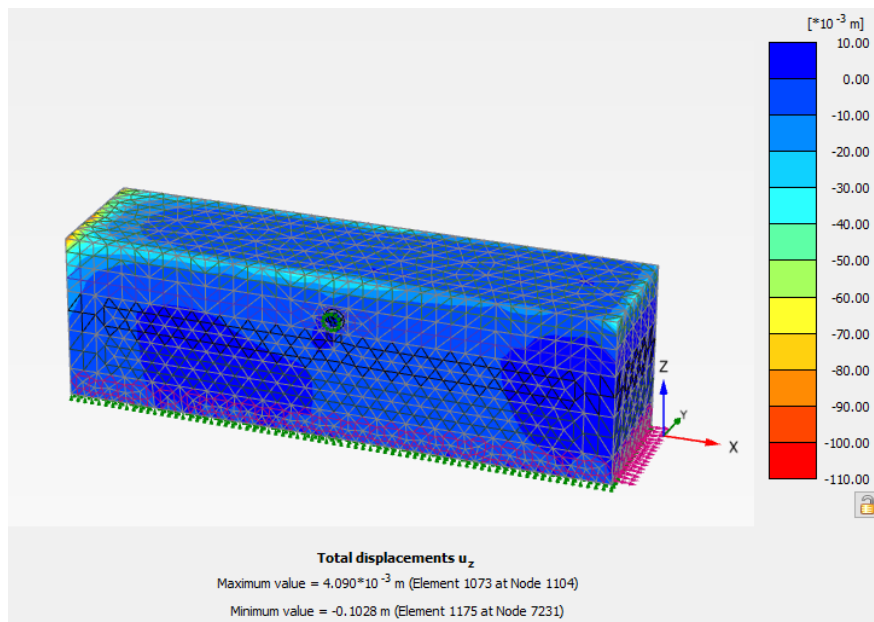


Figure 5. Vertical displacement contours after the earthquake.

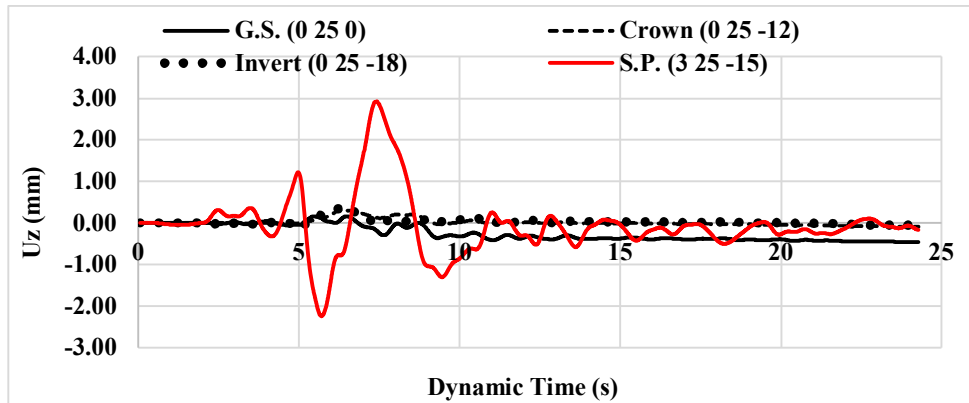


Figure 6. Vertical displacement at the different points,

**4.4. Longitudinal displacements**

After the end of the earthquake, Figure 7 shows the longitudinal displacement (in the Y direction) contours. The maximum longitudinal displacement was 55.77 mm in element 1057 at node 3788. The values of maximum longitudinal displacements,

$U_y$ , have also been presented in Table 4 for various critical locations, which again suggest that except at the ground surface, values of longitudinal displacement do not change much with respect to time. The time history of this longitudinal displacement has been plotted in Figure 8.

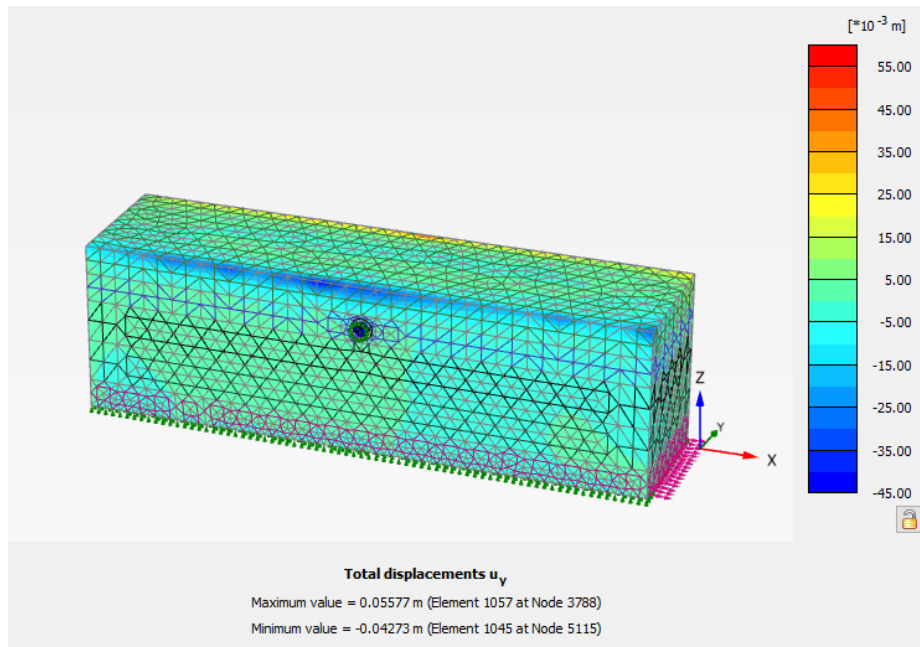


Figure 7. Contours of longitudinal displacement after the earthquake.

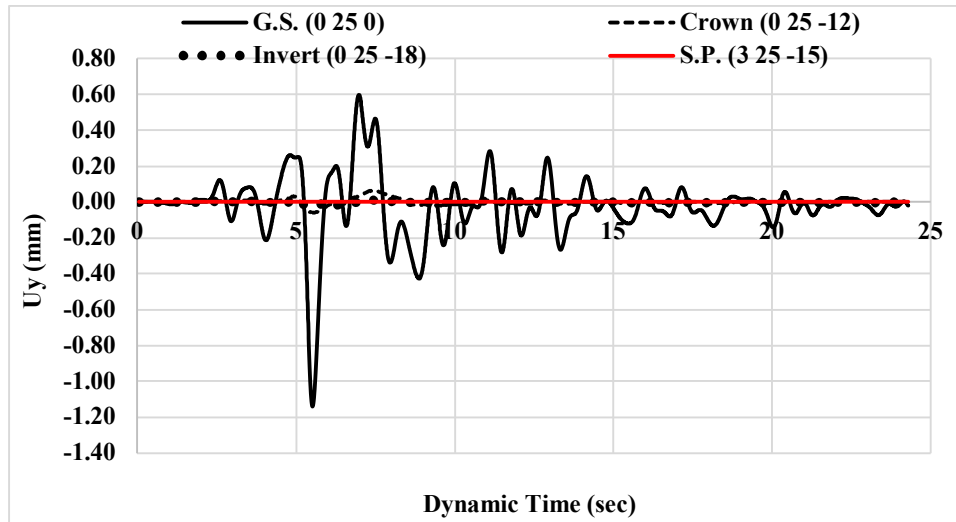


Figure 8. Longitudinal displacement vs. time history at the different points.

#### 4.5. Longitudinal Displacement Profile (LDP)

Figure 9 shows the longitudinal displacement (Y-direction) profiles at the ground surface along the length of the tunnel. The LDP profiles are presented for different time intervals. Longitudinal displacement is minimum at the mid-length of the tunnel between  $r = 10$  m and  $r = 40$  m, whereas

longitudinal displacement increases at both ends of tunnel. The longitudinal displacement is maximum at the near end; the maximum displacement is 32 mm at the time,  $t = 24.28$  s, which reduces to a negligibly small value at 10 m away. Near the far end, the longitudinal displacement increases from about 2 mm at 40 m to 41.27 mm at the far end.

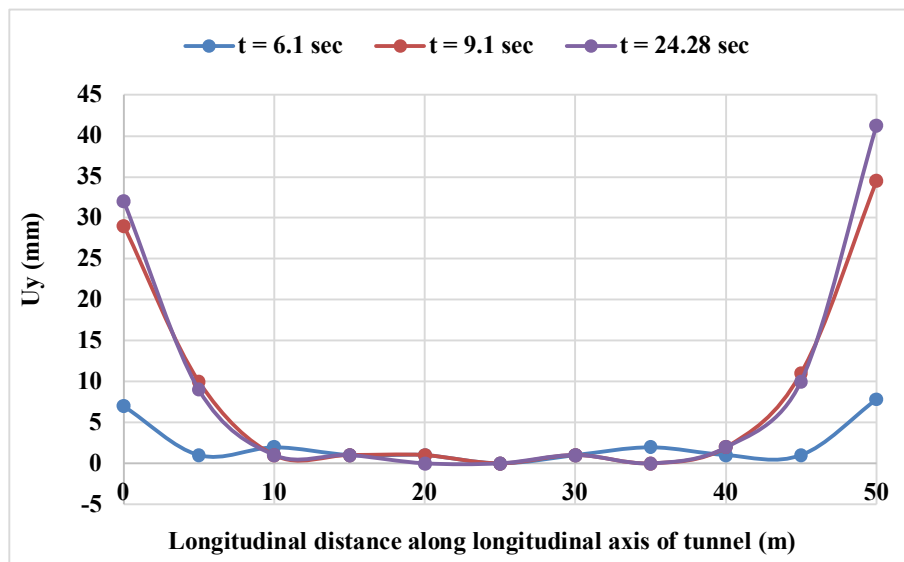


Figure 9. Longitudinal displacement profiles at the ground surface.

From Figure 9, it can also be observed that the longitudinal displacement profiles at the ground surface are much higher near the boundaries. This phenomenon happened due to the stress concentration and stress redistribution after the soil excavation. When a tunnel is excavated through the ground, it disrupts the natural stress distribution within the soil. This disturbance, especially near the tunnel's entrance, can result in stress

concentrations due to the interaction between the tunnel's lining and the surrounding soil. Consequently, this localized effect can lead to higher levels of deformation and increased displacement at the tunnel exit. Overall, the excavation process fundamentally alters the stress distribution within the soil mass, giving rise to zones of elevated stress and deformation,

particularly in close proximity to the tunnel's opening.

**4.6. Structural forces/ bending moment in RC liners**

The values of residual forces and bending moments in RC liners after the end of the earthquake have been tabulated in Table 5. Axial force and shear force increased after the earthquake, whereas there was a marginal increment in the bending moments.

**Table 5. Structural parameters in RC liners after the earthquake.**

Structural parameters of lining	Increment
N <sub>1</sub> (kN)	25.6
N <sub>2</sub> (kN)	1.2
Q <sub>12</sub> (kN)	7.7
Q <sub>23</sub> (kN)	4.8
Q <sub>13</sub> (kN)	3.5
M <sub>11</sub> (kN-m)	0.09
M <sub>22</sub> (kN-m)	2.8
M <sub>12</sub> (kN-m)	0.16

**4.7. Induced acceleration**

The values of maximum induced acceleration at various critical locations due to the horizontal component of acceleration have already been tabulated in Table 4. This table suggests that

induced acceleration is maximum at the mid-length of the tunnel for all components of the earthquake. The time histories of induced acceleration have been plotted in Figure 10 for different critical locations.

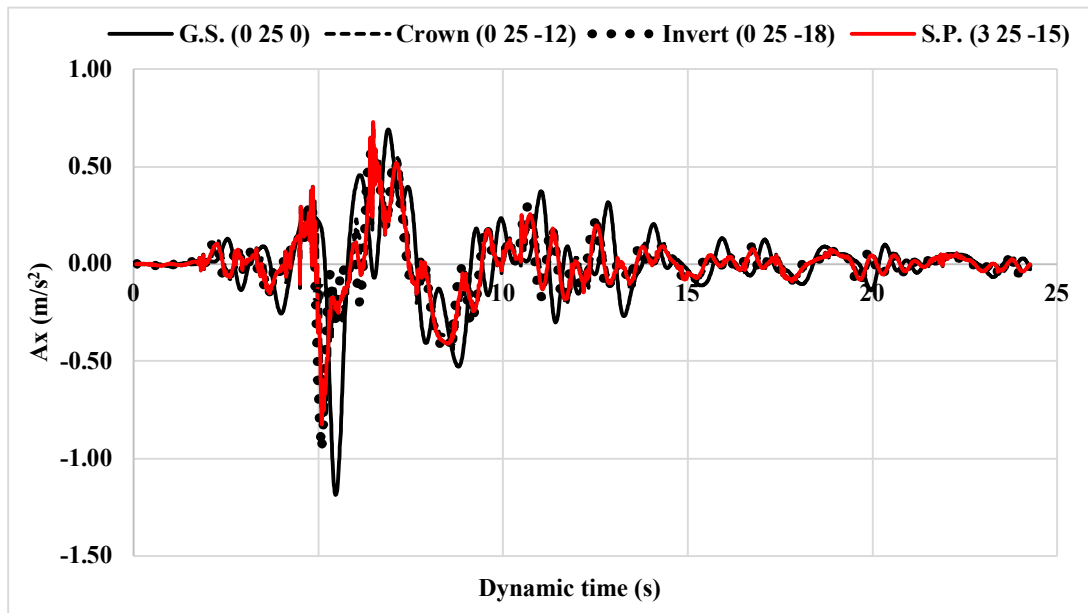


**Figure 10. Time history of horizontal acceleration caused by the T component of the earthquake at various locations.**

Maximum horizontal acceleration of 1.19 m/s<sup>2</sup> is experienced at the ground surface, with acceleration levels of 0.79 m/s<sup>2</sup> at the tunnel crown,

0.95 m/s<sup>2</sup> at the tunnel invert, and 0.82 m/s<sup>2</sup> at the springing points, respectively.

**4.8. Effect of boundary conditions on dynamic response**

Time histories of horizontal acceleration induced at the ground surface and crown of the tunnel due to earthquake have been displayed in

Figures 11 and 12, respectively. The absorbent boundary gives minimum horizontal acceleration, almost 50%, as compared to that by either the elementary or the free-field boundary. Horizontal acceleration is approximately the same for both elementary and free-field boundaries.

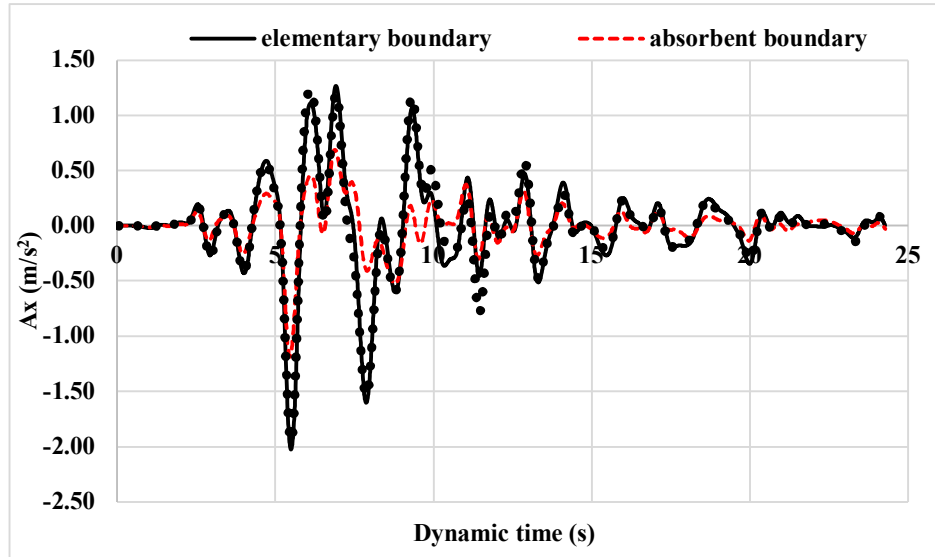


Figure 11. Effect of boundary conditions on horizontal acceleration at the ground surface.

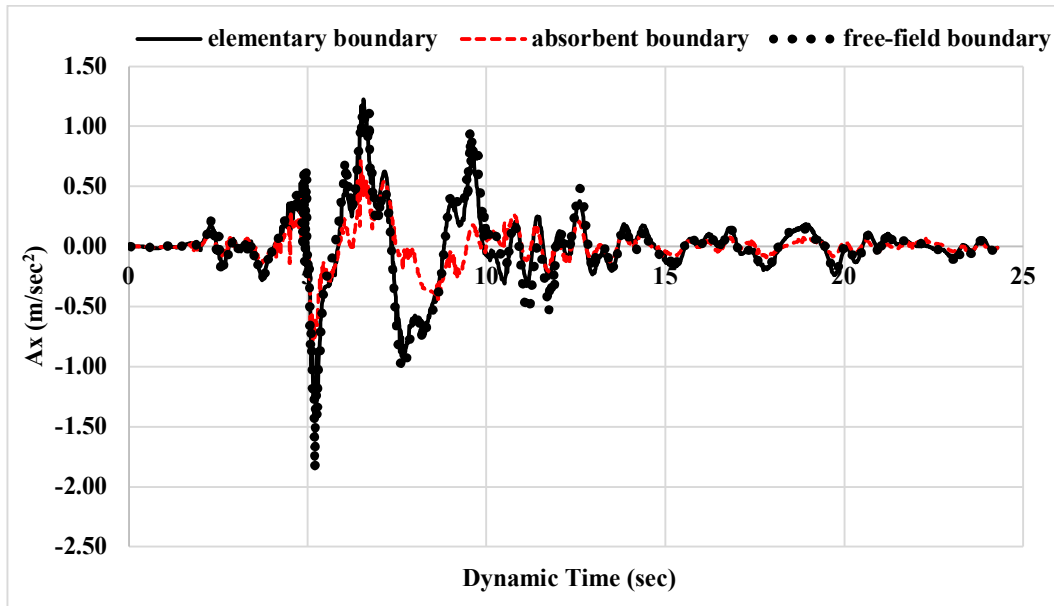


Figure 12. Effect of boundary conditions on horizontal acceleration at the crown.

Figures 13 and 14 depict the time histories of horizontal displacement at the ground surface and the tunnel's crown, respectively. Undoubtedly, the maximum horizontal displacement obtained by using the absorbent boundary is much smaller at both locations (206.39 mm at the ground surface

and 189.79 mm at the crown) as compared to 286.46 mm at the ground surface and 264.60 mm at the crown given by the elementary boundary or 320.87 mm at the ground surface and 298.62 mm at the crown as given by the free-field boundary.

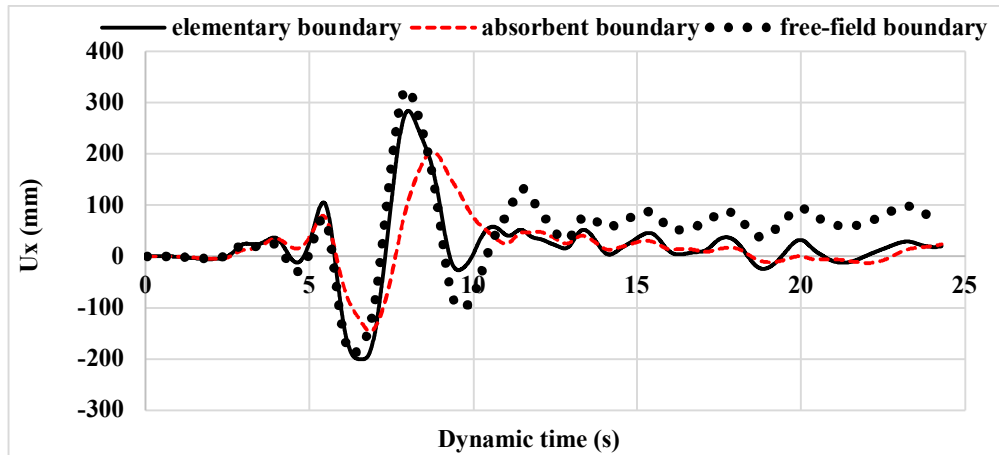


Figure 13. Effect of boundary conditions on horizontal displacement at the ground surface.

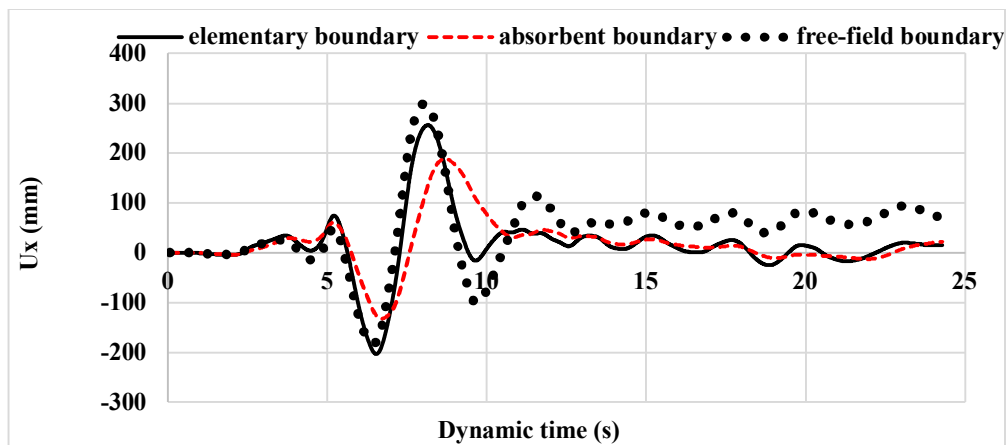


Figure 14. Effect of boundary conditions on horizontal displacement at the crown.

Similarly, Figures 15 and 16 clearly show that the values of both maximum longitudinal and vertical displacements obtained in the case of the absorbent boundary are much less than the corresponding values given by the other two boundaries. Absorbent boundaries showed the

most promising output as compared to the other boundary conditions. Therefore, absorbent boundary is suitable for dynamic analysis and the other two boundaries (free-field and elementary boundary) should not be used for the dynamic analysis.

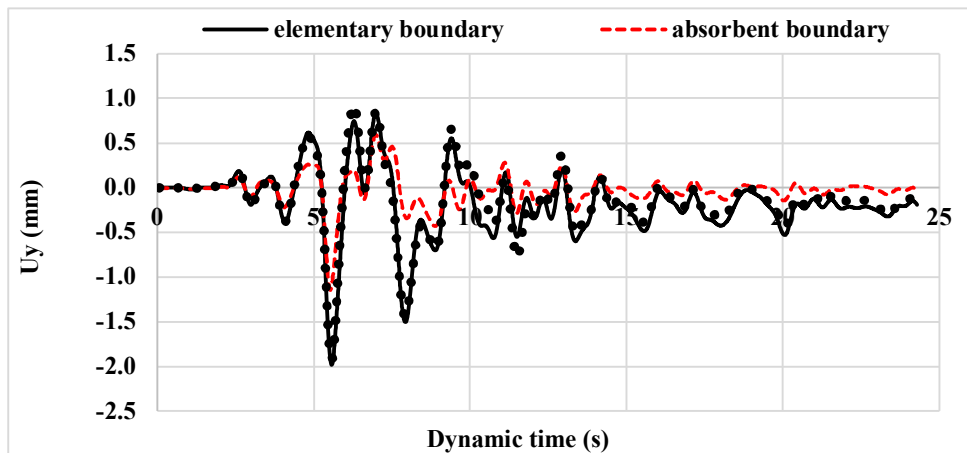


Figure 15. Effect of boundary conditions on longitudinal displacement at ground surface.

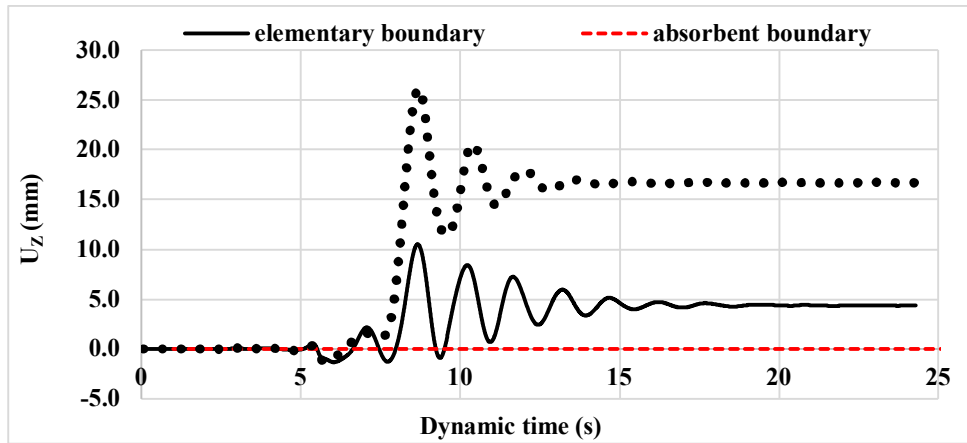


Figure 16. Effect of boundary conditions on vertical displacement at the ground surface.

**4.9. 3D analysis vs. 2D plane strain analysis**

The tunnel’s response in static conditions may be obtained by two-dimensional analysis (as a plane-strain problem) because the tunnel’s deformation along the length of the tunnel is negligible and can be ignored in static analysis. However, for dynamic analysis and for important structures the 2D numerical simulations do not offer results close to reality. Therefore, it is advisable to perform the three-dimensional analysis to obtain a true response in dynamic analysis. [26-38].

The dynamic response of a metro tunnel in three dimensions has been compared with the response

anticipated by a two-dimensional plane-strain analysis. The dynamic response is much lower in the 3D analysis compared to the 2D plane-strain analysis. Horizontal displacement and horizontal acceleration were found to be maximum in the case of 2D plane strain analysis (Table 6). However, the residual forces in RC liners have been found to increase at the end of the earthquake in 3D analysis (Table 7). The sign convention in Table 7 has been adopted from [39], according to which axial forces and shear forces are positive when they generate tensile stresses and vice-versa. Bending moment is defined as positive when it acts in a clockwise direction, and negative in a clockwise direction. [39].

**Table 6. Comparison of dynamic responses.**

Points	$(U_x)_{max}$ in mm		$(A_x)_{max}$ in $m/s^2$	
	2D plane strain analysis	3D analysis	2D plane strain analysis	3D analysis
G.S.	341	203.4	1.79	1.19
Crown	318	187.37	1.14	0.79
Invert	306	184.62	1.18	0.95
S.P. (1)	311	186.12	1.16	0.82
S.P. (2)	312	185.87	1.16	0.82

**Table 7 Comparison of structural parameters in RC liners**

Structural parameters of lining	T component of EQ	
	2D plane strain analysis	3D analysis
$\delta T$ (kN)	2.46	25.6
$\delta V$ (kN)	-0.27	7.7
$\delta M$ (kN-m)	-0.89	2.8

**5. Conclusions**

i) During the earthquake, maximum horizontal, vertical, and longitudinal displacements of the soil tunnel system were felt near the ground surface. The values of longitudinal displacement do not change

much with respect to time, except at the ground surface.

ii) Longitudinal displacement at the ground surface along the length of the tunnel is minimum at the mid-length of the tunnel, whereas it increases at both ends of the tunnel.

- iii) The increment in axial force and shear force of tunnel lining due to earthquake was greater than the increment in bending moment in tunnel lining.
- iv) The induced horizontal acceleration due to earthquake was maximum at the mid-length of the tunnel. Further, induced horizontal acceleration due to earthquake was maximum at the ground surface as compared to the tunnel's crown, tunnel's invert, and springing points of tunnel.
- v) In dynamic analysis, the absorbent boundary is much more effective in controlling the displacements as well as the induced acceleration than the elementary boundary or the free-field boundary.

## References

- [1]. Baron, M. L., Bleich, H. H., & Weidlinger, P. (1960). *Theoretical studies on ground shock phenomena* (p. 0215). Mitre Corporation.
- [2]. American Society of Civil Engineers. Engineering Mechanics Division. Committee on Structural Dynamics. (1964). *Design of structures to resist nuclear weapons effects* (No. 42).
- [3]. Biggs, J. M. (1964). Introduction to structural dynamics. (*No Title*).
- [4]. Li, P., & Song, E. X. (2015). Three-dimensional numerical analysis for the longitudinal seismic response of tunnels under an asynchronous wave input. *Computers and Geotechnics*, 63, 229-243.
- [5]. Varna, M., Maji, V. B., & Boominathan, A. (2022). Seismic Assessment of Shotcrete Support in Jointed Rock Tunnels. *International Journal of Geosynthetics and Ground Engineering*, 8(4), 51.
- [6]. Imteyaz, W., & Mishra, S. (2023). Stability Analysis of the Shallow Tunnel Under Soft Ground Regime. *Materials Today: Proceedings*.
- [7]. Zaid, M., Mishra, S., & Rao, K. S. (2020). Finite element analysis of static loading on urban tunnels. In *Geotechnical Characterization and Modelling: Proceedings of IGC 2018* (pp. 807-823). Singapore: Springer Singapore.
- [8]. Singh, M., Viladkar, M. N., & Samadhiya, N. K. (2017). Seismic response of metro underground tunnels. *International Journal of Geotechnical Engineering*, 11(2), 175-185.
- [9]. Shah, I. A., & Zaid, M. (2020, December). Behavior of underground tunnel under strong ground motion. In *Proceedings of Indian geotechnical conference (IGC 2020), Vizag, India*.
- [10]. Olarewaju, A. J., Rao, N. S. V. K., & Mannan, M. A. (2010). Response of Underground Pipes due to Blast Loads by Simulation- An Overview. *Electronic Journal of Geotechnical Engineering*, 15(H), 831-852.
- [11]. Alzabeebee, S. (2020). Seismic settlement of a strip foundation resting on a dry sand. *Natural Hazards*, 103(2), 2395-2425.
- [12]. Stamos, A. A., & Beskos, D. E. (1995). Dynamic analysis of large 3-D underground structures by the bem. *Earthquake engineering & structural dynamics*, 24(6), 917-934.
- [13]. Stamos, A. A., & Beskos, D. E. (1996). 3-D seismic response analysis of long lined tunnels in half-space. *Soil Dynamics and Earthquake Engineering*, 15(2), 111-118.
- [14]. Yu, H., Yuan, Y., & Bobet, A. (2017). Seismic analysis of long tunnels: A review of simplified and unified methods. *Underground Space*, 2(2), 73-87.
- [15]. Yu, H., Yuan, Y., Chen, Z., Yu, G., & Gu, Y. (2009). Full 3D numerical simulation method and its application to seismic response analysis of water-conveyance tunnel. In *Computational Structural Engineering: Proceedings of the International Symposium on Computational Structural Engineering, held in Shanghai, China, June 22-24, 2009* (pp. 349-358). Springer Netherlands.
- [16]. Chen, G., Li, T., Zhang, G., Yin, H., & Zhang, H. (2014). Temperature effect of rock burst for hard rock in deep-buried tunnel. *Natural Hazards*, 72, 915-926.
- [17]. Ichimura, T., Tanaka, S., Hori, M., Yamamoto, Y., Dobashi, H., Osada, M., ... & Yamada, T. (2016). Full three-dimensional seismic response analysis of underground structures with large complex cross sections and two-step analysis method for reducing the computational costs. *Journal of Earthquake and Tsunami*, 10(05), 1640016.
- [18]. Konstandakopoulou, F. D., Beskou, N. D., & Hatzigeorgiou, G. D. (2021). Three-dimensional nonlinear response of utility tunnels under single and multiple earthquakes. *Soil Dynamics and Earthquake Engineering*, 143, 106607.
- [19]. Li, Y., Di, H., Zhou, S., & Gong, Q. (2021). Seismic analysis for cross transfer subway stations in soft soil stratum. *Ksce Journal Of Civil Engineering*, 25, 1732-1745.
- [20]. Yadav, H. R. (2005). *Geotechnical evaluation and analysis of Delhi metro tunnels* (Doctoral dissertation).
- [21]. Soni, S. (2015). *Static and dynamic response of Delhi metro tunnels* (Doctoral dissertation, IIT Delhi).
- [22]. Plaxis 3D (2023), PLAXIS 3D 2023 reference manual. PLAXIS BV, Delft.
- [23]. Damians, I. P., Olivella, S., Bathurst, R. J., Lloret, A., & Josa, A. (2022). Modeling Soil-Facing Interface

Interaction With Continuum Element Methodology. *Frontiers in Built Environment*, 8, 842495.

[24]. Lysmer, J., & Kuhlemeyer, R. L. (1969). Finite dynamic model for infinite media. *Journal of the engineering mechanics division*, 95(4), 859-877.

[25]. Kumar, A. (2004, August). Software for generation of spectrum compatible time history. In *Proceedings of 13th world conference on earthquake engineering* (pp. 1-6).

[26]. Franzius, J. N. (2004). *Behaviour of buildings due to tunnel induced subsidence* (Doctoral dissertation, Imperial College London (University of London)).

[27]. Peck, B. B. (1969). Deep excavation and tunnelling in soft ground, State of the art volume. In *7th ICSMFE* (Vol. 4, pp. 225-290).

[28]. Attewell, P. (1978). Ground movements caused by tunnelling in soil.

[29]. Ozkaya, U., Melgani, F., Bejiga, M. B., Seyfi, L., & Donelli, M. (2020). GPR B scan image analysis with deep learning methods. *Measurement*, 165, 107770.

[30]. Soubra, A. H., Dias, D., Emeriault, F., & Kastner, R. (2008). Three-dimensional face stability analysis of circular tunnels by a kinematical approach. In *GeoCongress 2008: Characterization, Monitoring, and Modeling of GeoSystems* (pp. 894-901).

[31]. Mroueh, H., & Shahrouh, I. (2008). A simplified 3D model for tunnel construction using tunnel boring machines. *Tunnelling and Underground Space Technology*, 23(1), 38-45.

[32]. Bloodworth, A., & Bloodworth, A. G. (2002). *Three-dimensional analysis of tunnelling effects on*

*structures to develop design methods* (Doctoral dissertation, University of Oxford).

[33]. Kasper, T., & Meschke, G. (2004). A 3D finite element simulation model for TBM tunnelling in soft ground. *International journal for numerical and analytical methods in geomechanics*, 28(14), 1441-1460.

[34]. Liu, G., & Liu, G. (1997). *Numerical modelling of damage to masonry buildings due to tunnelling* (Doctoral dissertation, University of Oxford).

[35]. Nguyen, P. D. (2003). *Modélisation numérique des soutènements d'excavation* (Doctoral dissertation, Marne-la-vallée, ENPC).

[36]. Vitali, O. P., Celestino, T. B., & Bobet, A. (2018). 3D finite element modelling optimization for deep tunnels with material nonlinearity. *Underground Space*, 3(2), 125-139.

[37]. Jin, Y. F., Zhu, B. Q., Yin, Z. Y., & Zhang, D. M. (2019). Three-dimensional numerical analysis of the interaction of two crossing tunnels in soft clay. *Underground Space*, 4(4), 310-327.

[38]. Ramsheh, F. A., Rashiddel, A., & Dias, D. (2021, August). 3D numerical simulations of tunneling induced soil deformations. In *Journal of Physics: Conference Series* (Vol. 1973, No. 1, p. 012207). IOP Publishing.

[39]. Plaxis 3 D Reference Manual. Finite element code for geotechnical engineering. [https://communities.bentley.com/cfs-file/\\_key/communityserver-wikis-components-files/00-00-00-05-58/PLAXIS3DCE\\_2D00\\_V20.03\\_2D00\\_2\\_2D00\\_Reference.pdf](https://communities.bentley.com/cfs-file/_key/communityserver-wikis-components-files/00-00-00-05-58/PLAXIS3DCE_2D00_V20.03_2D00_2_2D00_Reference.pdf).

## تحلیل الاستو-پلاستیک سه بعدی تونل‌های زیرزمینی مترو دهلی تحت بارگذاری لرزه‌ای

### راهول شاکیا و مانندرا سینگ\*

گروه مهندسی عمران، موسسه ملی فناوری هامیرپور، هیمالچال پرادش، هند

ارسال ۲۰۲۳/۰۷/۱۰ پذیرش: ۲۰۲۳/۱۲/۰۷

\* نویسنده مسئول مکاتبات: manendra@nith.ac.in

---

#### چکیده:

با توجه به ماهیت بحرانی خطر لرزه‌ای در تونل‌های مترو، پاسخ لرزه‌ای تونل‌های زیرزمینی موضوع بسیار حساسی است. پاسخ لرزه‌ای یک سازه زیرسطحی بیشتر به خواص زمین اطراف و تغییر شکل زمین در هنگام زلزله بستگی دارد تا به خواص اینرسی سازه. این مقاله پاسخ لرزه‌ای یک بخش معمولی از تونل زیرزمینی شرکت راه‌آهن مترو دهلی (DMRC) بین میدان راجیو و میدان پاتل در محل کانات دهلی نو را بررسی می‌کند. تحلیل الاستو-پلاستیک سه بعدی تونل‌های زیرزمینی مترو دهلی تحت بارگذاری لرزه‌ای به روش اجزای محدود با استفاده از نرم افزار Plaxis 3D انجام شده است. علاوه بر این، تأثیر شرایط مرزی مختلف بر پاسخ دینامیکی تونل‌های مترو مورد بررسی قرار گرفته است. مقایسه تحلیل سه بعدی با آنالیز صفحه کرنش دو بعدی نیز انجام شده است. جابجایی‌های افقی در مقایسه با جابجایی‌های طولی و عمودی در سیستم تونل خاک، حداکثر تجربه شد. در تحلیل دینامیکی، مرز جاذب در کنترل جابجایی‌ها و شتاب القایی بسیار مؤثرتر از مرز ابتدایی یا مرز میدان آزاد است.

کلمات کلیدی: تونل زیرزمینی، FEM، Plaxis 3D، DMRC.

---